IEEE Access
Multidisciplinary | Rapid Review | Open Access Journal

Received 3 December 2022, accepted 20 December 2022, date of publication 23 December 2022, date of current version 5 January 2023.

Digital Object Identifier 10.1109/ACCESS.2022.3232063

APPLIED RESEARCH

Digital Twin-Based Monitoring System of Induction Motors Using IoT Sensors and Thermo-Magnetic Finite Element Analysis

JHENNIFER F. DOS SANTOS[1], BENDICT K. TSHOOMBE[1], LUCAS H. B. SANTOS[1], RAMON C. F. ARAÚJO[2,3], ALLAN R. A. MANITO[4], WELLINGTON S. FONSECA[1,3,4], AND MARCELO O. SILVA[3]

[1]Department of Electrical Engineering, Federal University of Pará, Belém 66075-110, Brazil
[2]Department of Theoretical and Experimental Physics, Federal University of Rio Grande do Norte, Natal 59078-900, Brazil
[3]Mechanical Engineering Graduate Program, Federal University of Pará, Belém 66075-110, Brazil
[4]Electrical Engineering Graduate Program, Federal University of Pará, Belém 66075-110, Brazil

Corresponding author: Ramon C. F. Araújo (ramon.araujo@itec.ufpa.br)

This work was supported in part by the Coordenação de Aperfeiçoamento de Pessoal de Nível Superior (CAPES/BRASIL) under R&D Project PROCAD-Amazônia, grant no. 88887.200548/2018-00.

ABSTRACT Electric induction motors are the type of motor most commonly operated in industry, and for this reason technologies that predict faults and reduce the corrective maintenance are of great interest. In this context, this paper presents a predictive maintenance tool of electric motors using the concepts of Digital Twin (DT) and Industrial Internet of Things (IIoT). The proposed system is innovative, as it monitors the motor current and temperature by means of sensors and a low-cost acquisition module, and these measurements are sent via Wi-Fi to a database. The concept of DT was leveraged by providing the measurements as inputs to a high-fidelity strongly-coupled model of the monitored monitor, using the Finite Element Method (FEM). The results obtained are satisfactory, because the sensors used presented acceptable errors that do not interfere with the reliability of the results. The computer simulation showed relative errors below 4% in the conductivity analysis and 10% in the temperature analysis. In addition, the simulation allows verifying the internal temperature of the motor, its resistive losses, and the intensity of the magnetic flux at each pole. It is worth pointing out that the internal analysis performed is only possible due to the combination of IIoT and computer simulations. Therefore, they allow a better diagnosis of the motor's operational status and also a time estimate for the next maintenance service, thus being ideal for the industrial sector.

INDEX TERMS Condition monitoring, digital twin, finite element analysis, induction motors, Internet of Things.

I. INTRODUCTION

Electric machines play a key role in modern society, especially in industrial operations. Used as the driving force for pumps, fans, compressors, conveyor belts, electric vehicles and other devices, electric machines are responsible for consuming 50% of the total energy generated worldwide [1], [2]. Among these machines, the induction motor is the most widely used in industry [3].

Like any other electromechanical device, induction motors are subjected to mechanical stress (e.g., vibration), thermal (heat) and electromagnetic stresses during operation [4], [5]. In the absence of proper maintenance, the motor progressively wears out and, eventually, a disruptive failure occurs. Failures represent large financial and operational losses due to unplanned corrective repairs and production downtime [6]. Therefore, great attention is paid to the maintenance of induction motors.

In recent years, the industry has been adopting the predictive maintenance approach, also called condition monitoring. In this paradigm, shutdowns for manual inspection and

The associate editor coordinating the review of this manuscript and approving it for publication was Taehong Kim.

repairs are performed with optimal periodicity, based on the actual current state of the equipment [7], [8]. In this way, outages are scarce when the equipment is in good working condition, and become more frequent in the end of its life cycle.

Predictive maintenance requires continuous monitoring of the equipment with sensors, in order to estimate its actual state [9]. In this context, the technology of monitoring systems has been positively affected by the emerging concepts of Internet of Things (IoT) and Digital Twin (DT), both fundamental to Industry 4.0 [10]. IoT is based on the networking of all objects [11]. When IoT is applied to industry, sensors are themselves connected to the Internet and measurements are sent to the cloud, from which they can be fetched and displayed to maintenance personnel in a convenient way for real-time remote monitoring. This application is called the Industrial Internet of Things (IIoT) [12].

The IIoT is connecting the physical world of sensors, devices and machines with the Internet, and by applying deep analytics through software, is turning massive data into powerful new insights and intelligence [13]. This advancement emphasizes extremely low latency, high reliability, security and privacy, and can handle large amounts of data. In addition, the core of IIoT is to widely connect devices to perform massive data collection and then use the algorithm models to perform in-depth data analysis to achieve broader value [14].

Another concept commonly found in Industry 4.0 is DT, which is the construction of a realistic computational model (virtual replica) of the monitored device by means of analytical methods and tools [15]. High-fidelity virtual models are usually achieved with Multiphysics numerical simulations, such as the one performed in [16], in which a structural coupling technique was used to model a power transformer under stressful operating conditions. With a digital twin it is possible, for example, to estimate the remaining device lifetime and to evaluate its behavior under certain operating conditions [17].

A Digital Twin is defined as a multi-physical, multi-scale, probabilistic, ultra-fidelity simulation that reflects, in time form, the state of the corresponding twin based on historical data, real-time sensor data, and physical model [18]. In this way, making it different from traditional simulations because the data used for simulation of the physical system is collected and recorded from the physical system space via IoT. This definition meets the main characteristics of the Digital Twin model to be demonstrated in this paper. The main technologies of the DT concept can be summarized into three categories, namely data related technologies, high fidelity modeling technologies and model-based simulation technologies [19], [20].

According to [21], data-related technologies are responsible for the process of data collection and transmission. They employ a lot of sensors, meters, readers, cameras, scanners, etc. However, the data that Digital Twins need is usually of large volume, high speed and great variety, which is difficult and expensive to transmit to the Digital Twin in the server cloud. Thus, pre-processing methods for the collected data are needed to reduce the network load and eliminate possible data leakage. One of the ideal methods for data preprocessing is edge computing [22].

Given this, DT can be leveraged to a large extent by IoT if the real-time data produced is used as input to build the Digital Twin model. The use of IoT and DT for monitoring is promising because it allows predictive maintenance to be applied to a variety of assets using fewer personnel, as well as to provide more information about the device that cannot be collected by sensors.

Applied to factories, this technology involves the collection and analysis of equipment data in real time, bringing several benefits. The collected information is made available to a user in a friendly way anywhere in the world through dashboard visualization (dashboards) implemented in web pages or mobile applications (for tablets/smartphones). Better tracking of industry assets allows for more assertive decision making, assistance in predictive maintenance of equipment and production optimization [23], [24].

Given the potential gains of this tool, many works have been published on induction motor monitoring [25], [26], [27]. The workflow of IoT-based monitoring is to employ a microcontroller to read the analog measurements collected by sensors and, via a Wi-Fi module, to send the digitized data to an IoT-cloud provider over the Internet [25], [26]. In addition, the authors of [27] have also developed algorithms that estimate the operating state of the machine by analysis of simple characteristics of the power supply current waveforms. However, these works do not use finite element analysis methods like the one proposed in this paper, which would result in more realistic models.

Other recent works using DT and IoT for fault prediction are [28] and [29]. At [28] introduces a system capable of identifying combined faults of a rotating machine and predicting faults, in a non-invasive machine manner. This identification is done using different machine learning techniques – namely support vector machines, k-nearest neighbors and random forests – where they are compatible for classification purposes. In the paper of [29], an IoT platform for real-time monitoring and remote visualization of power substations is proposed. In the work [30], neural networks are used by MATLAB/Simulink software that monitors performance and performs remote prognostics of electric motor health in real time through the cloud, which is made the Digital Twin through simulations using the finite element method. Furthermore, a paper recently published by the authors in [1] proposes a monitoring based on DT system that numerically models the monitored motor using only input current measurements.

In this scenario, the main contribution of this work is the use of the Finite Element Method (FEM) for the computational development of a induction motor Digital Twin, considering a strong numerical coupling thermo-magnetic simulations [31]. Additionally, an IIoT system is used, which provides motor's parameters (current and temperature) as input data for the computer simulation. Moreover,

improvements are also implemented in this work in order to achieve more accuracy results, such as: additional monitored variable (temperature), offering a better accuracy of the virtual motor model developed in FEMM and, consequently, a better analysis of the real motor conditions considered; validation of the motor's parameters mentioned above, aiming to obtain more reliable measurement values for the proposed system. In addition, new results were obtained such as the validation of the motor current and temperature sensors, resistive losses analysis in the stator and rotor, simulated temperature analysis in the rotor and stator of the machine, and analysis of the conductivity of the motor windings.

The methodology of this paper is described as follows: Thermal and current sensors are used to measure the temperature and input current of a motor, respectively. Connected to the sensors is a microcontroller that samples and digitizes the measurements. Next, a Wi-Fi sends the digital data to a cloud platform, where it is stored in databases. The measurements stored in the cloud are accessible on the Internet via a web page. Furthermore, the measured data stored in the cloud are used as inputs to a numerical Finite Element Model simulated in FEMM (Finite Element Method Magnetics) software [32] to achieve a virtual replica of the motor according to the Digital Twin concept. The purposes of the numerical simulations are to realistically reproduce the operation of the monitored motor and to obtain extra information that is not collected by sensors, allowing one to have a deeper understanding of the monitored device condition in a non-invasive way.

II. THE MOTOR MONITORING AND ANALYSIS SYSTEM

In the context of this article, a DT application is designed to perform the monitoring of industrial electrical equipment and transmission of the measured data via the internet to users in control of the industrial operation. The project described in this document is hereafter called Motor Monitoring and Analysis System (from Portuguese, Sistema de Monitorização e Análise de Motores - SMAM).

Fig. 1 shows the architecture of the SMAM system which comprises of four stages, namely the electrical machine being monitored, current and temperature acquisition cloud storage and post-processing of data through Finite Element Analysis (FEA) and real-time graphs. In brief terms, there are sensors connected to the motor continuously measuring the temperature on its frame and feed current.

An IoT microcontroller samples the sensor readings at regular time intervals and sends the digitized data through a Wi-Fi access point to a cloud platform. The sent data are stored in a database in the cloud, and are accessible in real-time through a web page for visualization and further analysis by the end-user. This data is used as input for the computer simulations.

A. INDUCTION MOTOR

In this project, a three-phase 1.1 kW induction motor (parameters in Table 1), connected in delta, is monitored. Its shaft is connected to a Foucault brake (also called eddy current brake), which acts as the mechanical load. The Foucault brakes consist of an aluminum plate and current coils. The coils' DC current is varied through a potentiometer, hence producing varying Foucault currents in the aluminum plate. These eddy currents produce a magnetic field opposite to the rotation of the motor axis [33], acting as a brake for the motor. In section IV, the motor will be subjected to different loads by varying the current on the Foucault coils.

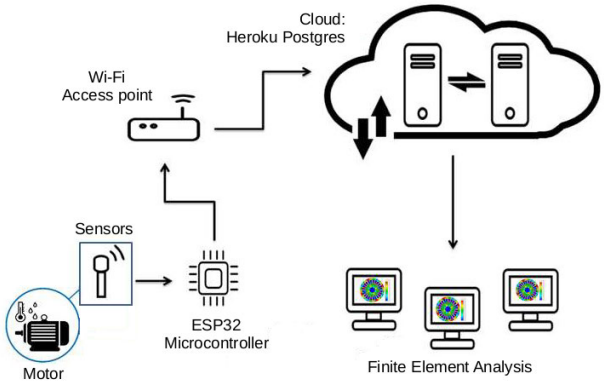

FIGURE 1. The framework of the implemented monitoring system.

TABLE 1. Parameters of the induction motor.

Parameter Description	Value
Efficiency class	IE2 Class
Nominal power	1.1 kW / 1.5 cv
Number of phases	3
Voltage	220 V
Nominal current	4.42 A
Nominal speed	1715 rpm
Power factor	0.80
Frequency	60 Hz

B. CURRENT ACQUISITION

The motor supply current is monitored in one phase in the IoT device, consisting of the following components: clamp current sensor SCT-013, signal conditioning circuitry and ESP32 microcontroller. The SCT-013 is a non-invasive sensor that measures AC currents up to 100 A. It is based on the electromagnetic induction effect [33], where the magnetic field of the phase current induces a proportional current in the sensor clamp. The split-core current transformer is composed of ferrite in the core and a dielectric strength of 1000 V between the shell and the output, in addition to the nominal input current range between 10% up to 120% and the supportable operating temperature of -25°C up to 70°C [34].

The sensor signal passes through a passive circuit (Fig. 2a) to be conditioned to a form suitable for being read by ESP32 accurately, spurious oscillations are filtered out and amplification is performed to levels within the controller's range. The conditioned signal is displayed on the ESP32's analog pins, digitized, and sent to the cloud via Wi-Fi. The ESP32 samples the current signal every second.

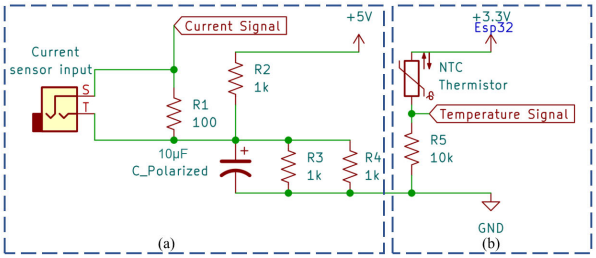

FIGURE 2. Diagrams of the (a) current and (b) temperature signal conditioning circuits. Nodes pointed by labeled balloons indicate the points at which the voltage signal is sampled by ESP32's analog pins.

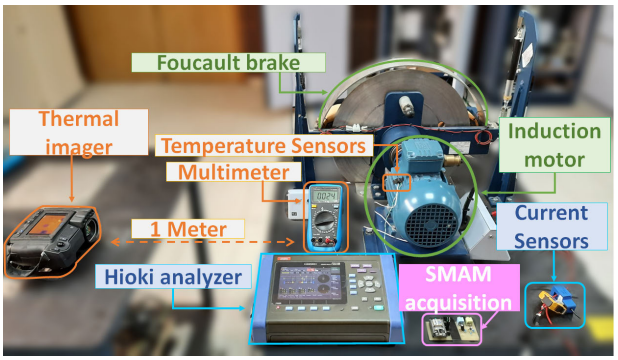

FIGURE 3. Setup of the motor's feed current and temperature measurement by SMAM and reference equipment (Hioki, multimeter and thermal camera).

A Hioki power quality analyzer was also installed to measure the supply current on the same phase monitored by the ESP32. This is a class A commercial equipment according to IEC 61000-4-30 [35]. The current from the analyzer is used as reference data, that is compared with the measurements from the proposed acquisition system for adjust and validation purposes. The Hioki analyzer is configured to sample the current signal every second. Fig. 3 shows the overall configuration of the measurements with the induction motor and the two current measurement systems (SCT-013 current sensor and Hioki analyzer).

Before the SMAM is deployed, the SCT-013 sensor must be calibrated in a preliminary round of measurements, using readings from other equipment as a reference. In this article, such equipment is the Hioki analyzer. The Hioki and the SMAM are set to measure the motor supply current on the same phase. By varying the current in the eddy coils, the motor is subjected to four increasing loads, one at a time and for five minutes each. Current data is recorded throughout the experiment, including the load transitions. Fig. 4 illustrates the current signals measured by the two sensors during the calibration phase.

The current samples recorded at the same time by Hioki and SMAM are plotted against each other; the SMAM measurements are associated with the horizontal axis. The result,

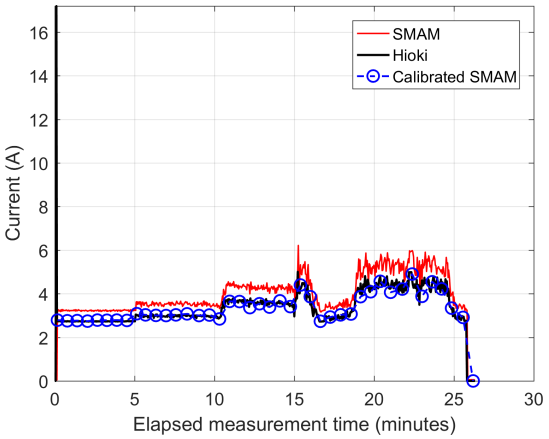

FIGURE 4. Preliminary calibration of SMAM's current sensor. Feed current measured by Hioki and by SMAM (before and after calibration).

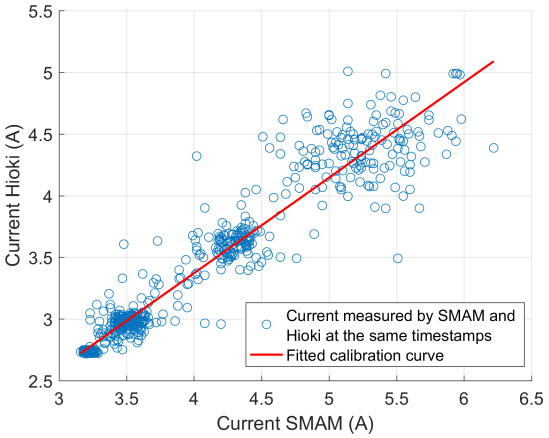

FIGURE 5. Fitting of calibration function.

shown in Fig. 5, is an illustration of the relationship between the readings from two sensors that capture the same event (current in the same phase) over time. A linear function is fitted to the points using the method of least squares. This is a calibration function whose input is the raw current reading from the TCS and the output is what the reference equipment would read if it were measuring the same current at the exact instant.

Once installed, the calibration function equation is implemented in the ESP-32 software in order to correct the SMAM current measurements in the implementation phase. The blue curve in Fig. 4 shows the SMAM measurements corrected with the fitted function from Fig. 5, and the close agreement with the Hioki data is evidence of a successful calibration procedure.

C. TEMPERATURE ACQUISITION

In addition to the supply current, the SMAM also monitors the temperature on the motor case side. The sensor used is an NTC (Negative Temperature Coefficient) thermistor. The MF52 series NTC thermistor is coated with an etoxylin resin and interconnected by a copper wire, where the rated power

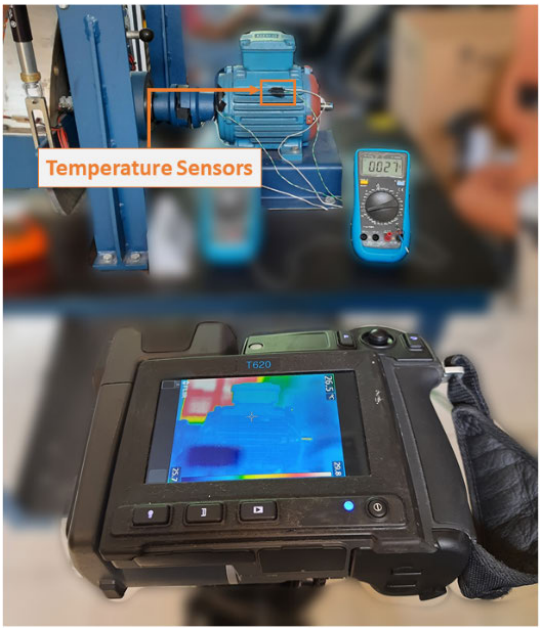

FIGURE 6. Temperature sensors and FLIR thermographic camera setup.

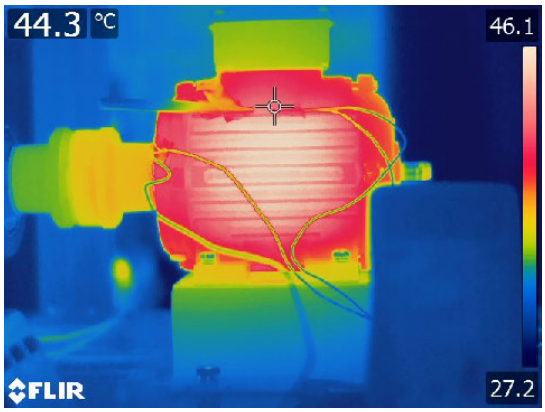

FIGURE 7. Example of thermal image captured by FLIR camera.

is close to 50 mW and a temperature range from −55 °C to 125 °C [36].

A known resistor is connected in series with the NTC to form a voltage divider, as shown in Fig. 2b. The voltage across the resistor is read by the ESP32's analog pins. The microcontroller code calculates the resistance of the NTC using the ratio of the voltage divider circuit and calculates the temperature from the resistance using the Steinhart-Hart equation.

For validation, the temperature is also measured by a thermocouple connected to a multimeter (Minipa model ET2042E) and a thermal camera (FLIR T620). Fig. 6 shows the temperature-related part of the measurement setup. The thermocouple and NTC sensors are attached to the side of the motor housing; care was taken to ensure that the sensors always touch the motor surface for accurate readings. The thermal camera is positioned at a distance of 1 meter from the engine, and its image is focused on the insulating tape holding the other sensors. The camera was set up with emissivity = 0.94, the same value for the insulating tape.

The temperature readings are recorded in different ways for the three sensors. The SMAM continuously sends samples to the cloud. The thermocouple measurement is recorded manually and from the thermal camera a thermographic image is captured, of which an example is shown in Fig. 7. Preliminary measurements with all three devices revealed that no calibration of the NTC sensor was necessary.

D. COMMUNICATION WITH THE WEB SERVER AND DATA STORAGE IN THE CLOUD

In this work, communications with the web server are performed using the HTTPS (Hypertext Transfer Protocol Secure) protocol since HTTPS has encrypted credentials, such as: SSL (Secure Socket Layer) and TLS (Transport Layer Security), they are responsible, in the whole process of sending, for the security of data against espionage and tampering [37]. Thus, this type of encryption was used for connection between the server and the developed system, because there is a concern with data security to avoid unwanted intrusions into the confidential information of the industry, thus avoiding problems in the production system.

For the exchange of messages with the server was chosen the JSON model, because its format is intended to be a language of easy computational and human reading [38]. The web server defined was the Heroku Postgres cloud platform, a free, online database service that internally uses PostgreSQL database technology [39]. After sampling the measurements collected by the temperature and current sensors, the ESP32 microcontroller sends the digitized data to Heroku Postgres by calling the HTTP POST method. The data received by Heroku is accessible through a specific web page, where the end user can monitor the measurements in real time. The information is secure because only selected users who have received the web page link can access the data.

In addition to being able to view the stored measurements, the end user can also schedule data retrieval for further analysis by issuing GET requests (an HTTP method) to Heroku. After sampling the measurements collected by the temperature and current sensors, the ESP32 microcontroller sends the data via Wi-Fi following the IEEE 802.11 communication protocol.

According to the manufacturer's specifications [40], the module supports a data rate of up to 150 Mbps and 20 dBm of output power at the internal antenna, has internal 32-bit (dual core) processors operating at 240 MHz and analog-to-digital converters. In addition, it features a 1 kHz sampling rate and floating point operations of the MFLOPS (million floating point operations per second) type [41]. Thus, being sufficient for the desired communication in the SMAM project, eliminating the need to attach an external antenna to transmit the

information. This feature ensures a wide physical range for data transmission.

The measurements made by the ESP32 are sent to Heroku Postgres. The quality of the signal sent can be indicated by the bit error rate (BER) which is based on the signal strength [42]. In the transmission of information, between the microcontroller and the Heroku server, this rate is low and is proven by the successful calibration of the SMAM sensors that is described in topic II-B.

III. FINITE ELEMENT FORMULATION FOR THERMO-MAGNETIC COUPLED PROBLEMS

The Finite Element Method (FEM) is a numerical technique used to obtain approximate solutions to boundary value problems in Engineering. The domain of analysis is discretized into a finite number of small parts (called elements), and in each of those elements an algeberaic approximation of the governing equation is set up. The set of equations formed in all elements form a global system of equations, which is calculated to solve for the unknown field(s) throughout the domain of analysis [43].

Before the global system of equations is calculated, boundary conditions need to be imposed on the solution domain. The two most important boundary conditions in FEM are the Dirichlet and periodic.

A high-fidelity, FEM-based model of the induction motor was built in this work using the FEMM (Finite Element Method Magnetics) software, widely used in literature. The inputs to FEMM are only the motor's geometry and a few easy-to-measure parameters such as phase current and temperature on the motor frame, excluding the massive amounts of data needed by deep learning based techniques proposed in other works. In the preprocessing phase of the simulations, FEMM solves four types of physics problems: magnetic, electrostatic, heat flow and current flow. This artifice occurs for solving Maxwell's equations.

In this paper, the realistic operation of the induction motor was simulated numerically, considering the strong coupling (two-way interdependence) between thermal and magnetic effects based on the work [44]. To process this simulation, FEMM needed to solve equations regarding low frequency electromagnetic models and Thermal Formulation described in the subsection below.

A. LOW-FREQUENCY ELECTROMAGNETIC MODEL

A detailed mathematical model is given in [43] on the FEM formulation and thus our focus will be on Maxwell's equations in the form solved by software FEMM [45]. Two important Maxwell's equations are the Faraday-Lenz and Ampère laws, which, in the low-frequency approximation, are respectively written as [33]

$$\nabla \times \boldsymbol{E} = -\frac{\partial \boldsymbol{B}}{\partial t} \tag{1}$$

and

$$\nabla \times \boldsymbol{H} = \boldsymbol{J} = \boldsymbol{J}_c + \boldsymbol{J}_{\text{src}}, \tag{2}$$

where $\boldsymbol{E}$ is the electric field vector, $\boldsymbol{H}$ the magnetic field, $\boldsymbol{B}$ the magnetic flux density, $\boldsymbol{J}_c$ and $\boldsymbol{J}_{\text{src}}$ are the conduction and imposed (by an external source) current densities, respectively. The conduction current density is related to the electric field according to Ohm's law

$$\boldsymbol{J}_c = \sigma \boldsymbol{E}. \tag{3}$$

The magnetic constitutive relation is also of interest:

$$\boldsymbol{B} = \mu(\boldsymbol{B})\boldsymbol{H}, \tag{4}$$

where $\mu(\boldsymbol{B})$ is the medium's magnetic permeability (function of $\boldsymbol{B}$ for nonlinear materials). Due to its zero divergence ($\nabla \cdot \boldsymbol{B} = 0$), $\boldsymbol{B}$ can be associated to a magnetic vector potential $\boldsymbol{A}$ as follows:

$$\boldsymbol{B} = \nabla \times \boldsymbol{A}. \tag{5}$$

Substituting (5) into Faraday's law yields:

$$\nabla \times \boldsymbol{E} = -\nabla \times \frac{\partial \boldsymbol{A}}{\partial t}, \tag{6}$$

which, in the case of 2-D problems, can be integrated to result in

$$\boldsymbol{E} = -\frac{\partial \boldsymbol{A}}{\partial t} - \nabla V. \tag{7}$$

In (7), the ∇V term is an additional voltage gradient that, in 2-D problems, is constant over a conducting body. This gradient is used by FEMM in harmonic problems to enforce constraints on the current carried by conductive regions. By substituting a convenient combination of equations (3), (4), (5), (7) into (2), we obtain.

$$\nabla \times \left(\frac{1}{\mu(\boldsymbol{B})} \nabla \times \boldsymbol{A}\right) = -\sigma \frac{\partial \boldsymbol{A}}{\partial t} - \sigma \nabla V + \boldsymbol{J}_{\text{src}}. \tag{8}$$

Equation (8) is solved in phasor form by software FEMM for time-harmonic magnetic problems.

By dimensional analysis, each additive term at the right-hand side of (8) is a form of current density. Defining the first term as

$$\boldsymbol{J}_e = -\sigma \frac{\partial \boldsymbol{A}}{\partial t}, \tag{9}$$

One can interpret that, apart from the gradient term, there are two types of electric currents involved in induction motors: source current in the stator armature $\boldsymbol{J}_{\text{src}}$ and the current induced $\boldsymbol{J}_e$ by the rotating magnetic field. During simulations, the resistive losses (q) due to current flow through the copper strands are calculated [46].

$$q = \frac{1}{\sigma} J^2. \tag{10}$$

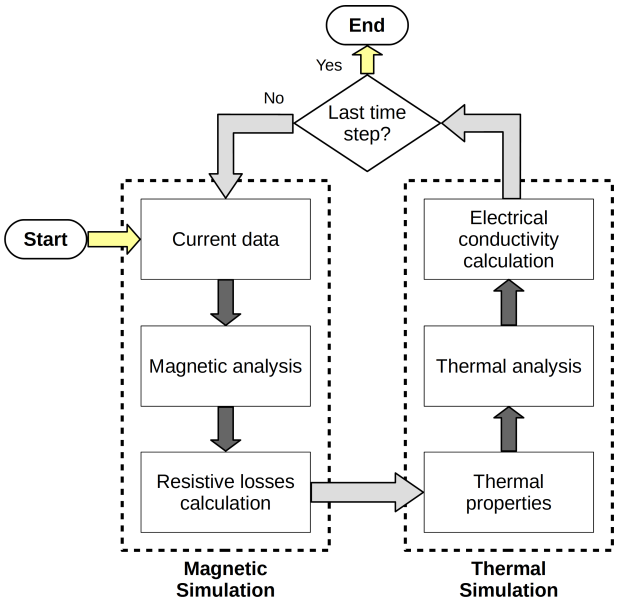

FIGURE 8. Algorithm for numerical simulations with strong thermo-magnetic coupling.

B. THERMAL FORMULATION

The thermal formulation solves the problem of transient heat conduction, governed by the equation [45]

$$\rho\, c_p \frac{dT}{dt} - \nabla \cdot (k \nabla T) = q, \tag{11}$$

where ρ is the mass density, c_p the specific heat capacity, k the thermal conductivity and T temperature. Equation (11) is solved by software FEMM by discretizing time with Euler's implicit discretization scheme. After calculating the temperature values at all the finite elements of the analysis domain by numerically solving (11), software FEMM updates the values of electric conductivity using the equation [46]

$$\sigma(T) = \frac{1}{\rho_0 (1 + \beta_0) T}, \tag{12}$$

where ρ_0 is the electrical resistivity at 0°C and β_0 the rate of variation of resistivity with temperature.

C. ALGORITHM FOR STRONG THERMO-MAGNETIC COUPLING

The multiphysics coupling was obtained from the pyFEMM package that allows simulations to be performed in FEMM from the Python programming language. The code consists of calculations that are performed iteratively over time, where each iteration is composed of a magnetic simulation and followed by a thermal simulation. Fig. 8 shows the block diagram of the coupling algorithm used.

As illustrated in Fig. 8 the output of each simulation is used as the input of the other to obtain a strong coupling, this type of interaction is able to faithfully represent the simulated physical phenomenon [47], [48]. At the beginning of each iteration, the magnetic simulation is run, in which equation (8) is solved numerically to calculate the potential

```
a_cu = 0.0040 # declared variables
ro_cu = 1/(58*1e6)
t1 = 5 ; aux = 0;
cond_est.clear();  t_estator.clear();
for j in range(1, 37): # stator coordinates
  m = (j-1)*10
  theta1 = t1 + m
  x1 = 5.3278*math.cos(theta1*degrau)
  y1 = 5.3278*math.sin(theta1*degrau)
  # conductivity calculation
  femm.ho_seteditmode("area")
  femm.ho_selectblock(x1,y1)
  aux3 = femm.ho_blockintegral(0)
  aux2 = aux3[0]
  t_estator.append(aux2)
  femm.ho_clearblock()
  aux = 1/(1e6*(ro_cu*(1+a_cu*(aux2-300))))
  cond_est.append(aux)
```

FIGURE 9. Code snippet (in Python) for calculating the stator conductivity from the numerical data generated in FEMM simulations.

```
# startup
femm.openfemm()
if i != 1:
  femm.opendocument("temp.fem")
# modification of conductivity values
# stator
for j in range(36):
  name = "Copper_"+str(j)+"_stator"
  femm.mi_modifymaterial(name, 5, cond_est[j])
#rotor
femm.mi_modifymaterial("Aluminum_rotor", 5,
                       cond_enr_rotor[i-2])
```

FIGURE 10. Code snippet (in Python) for modifying the parameters of motor materials modeled in FEMM simulations.

of the magnetic vector A in all finite elements that form the analysis region. In addition, the resistive losses in the copper strands are calculated using equation (10).

Next, the thermal simulation is started where equation (11) is solved numerically on all finite elements, using the resistive losses calculated in the previous magnetic simulation as heat sources. The electrical conductivities are updated at the new temperatures according to (12). To do this, it is necessary to state equations (11) and (12) in the code, in addition to the geometric coordinates of each part of the stator and rotor. In Fig. 9 the realization of this process in the developed program is illustrated.

The calculated values are stored and reintroduced into the magnetic simulation of the next step by means of the repeat present in the code. The condition set in this repetition updates the conductivity values with the mimodifymaterial function as illustrated in Fig. 10. This process is repeated until the simulated time period is complete.

D. POST-PROCESSING OF DATA USING FINITE ELEMENT ANALYSIS (FEA)

As the main contribution of this work, the monitored equipment is also numerically simulated using the measured temperature and the the current as inputs. With the numerical model, it is possible to obtain information that is not provided by the sensors, for example resistive losses in the stator and rotor, in order to better understand the state of the monitored device. The idea is to accurately reproduce the current operating conditions of the motor with numerical models, which

TABLE 2. Electric parameters of materials used in FEMM simulation.

Material	Component(s)	Relative Permeability	Electrical Conductivity (MS/m)	Thermal Conductivity (W/m.K)
Aluminum	Rotor armature	1	34.45	84
M-45 Steel	Rotor and Stator core	4689	2.90	52
Air	Air gap	1	0	0.03
Copper	Stator armature	1	58	70

allows a complete analysis of its behavior and condition without the need to shut down the motor or install invasive sensors.

The open source software FEMM (Finite Element Method Magnetics) is used in simulations and the following data are required as inputs: the geometric model, boundary conditions, electromagnetic material parameters and supply current. The Galerkin boundary condition (A=0) is used. The electromagnetic parameters of the modeled motor parts are listed in Table 2.

To perform the thermal-magnetic coupling using FEM, the following data are required as input: total losses obtained from the magnetic simulation in the thermal simulation, the material according to its thermal properties obtained from [31], convection boundary condition, also specifying the thermal conductivity (W/m.K) and the ambient temperature. The simulation feed-in current and ambient temperature are based on the values measured by the corresponding sensors, obtained from the database. Relatively the mesh used contained 92294 triangular elements and 46426 nodes.

IV. RESULTS

A. MONITORING PHASE CURRENT AND TEMPERATURE ON THE MOTOR FRAME AT DIFFERENT LOADS

The acquisition setup described in section II was employed to monitor the feed current and temperature of the induction motor. Notice that the measurements reported here took place after SMAM's current sensor was calibrated according to the procedure of section II-B e II-C.

By varying the current of Foucault coils with the potentiometer, the motor was subjected to four load levels successively, for five minutes each. In this study we will refer to those loads as I, II, III and IV. At load I there is no current into the Foucault coils, there is only the inertia of the Foucault brakes. At loads II, III and IV the current into the Foucault coils is 3 A, 3.5 A and 4 A, respectively.

The current data collected by Hioki and SMAM's calibrated sensor are illustrated in Fig. 11. The initial peak, as 20.33A measured by SMAM and 17.90A measured by Hioki, is due to the direct on-line starting of the motor. After that, the motor enters steady-state regime with small jumps in current, considering five minutes apart from each other, which correspond to the load levels being applied successively.

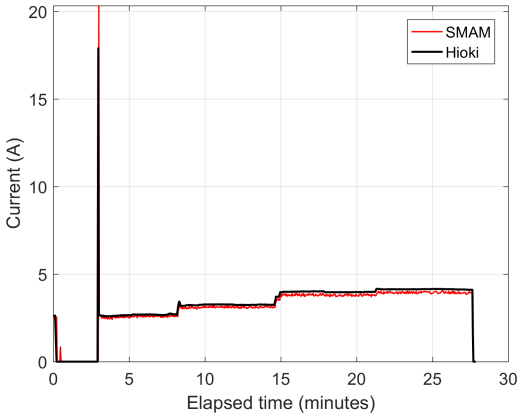

FIGURE 11. Motor's phase current at different load conditions, as measured by Hioki and SMAM devices.

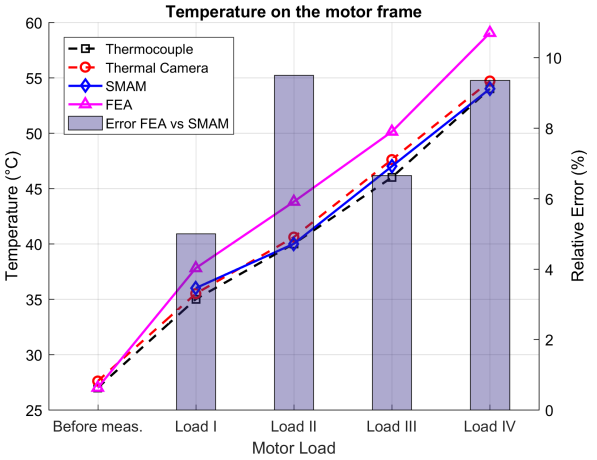

FIGURE 12. Simulated and measured values of temperature on the side of the motor frame.

There is good agreement both in transient and steady-state regimes, with the error of SMAM's readings relative to Hioki equal to 13.6% for the starting peak and 4.4% on average during steady state. The relatively low errors for the current measurements of SMAM demonstrate that it is possible to use low-cost sensors to leverage the benefits of IoT and DT on a large scale, with little compromise of accuracy.

During the experiment, besides current, temperature on the side of the motor casing was also monitored by SMAM, thermocouple and thermal camera. After the motor has been running for five minutes under each load level, the temperature readings of the thermocouple and thermal camera were manually captured and compared to with the NTC values at that same time instant. The strongly coupled thermo-magnetic model of the induction motor was also simulated in FEMM software to obtain simulated values of temperature.

Fig. 12 shows the simulated and measured temperatures on the side of the motor casing. All values start close to 27°C, which was the room's ambient temperature before measurements began. It is observed for all sensors the pattern of rising temperature as load levels increase, which is expected as the higher motor current dissipates more heat. For all load levels

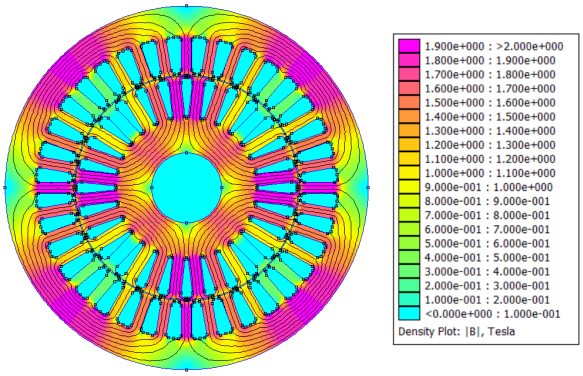

FIGURE 13. Simulated magnetic flux density in the induction motor.

the temperature measured by the sensors are very close to each other. The simulated values tended to be higher than the measured ones, in part because the effect of heat exchange with air was not taken into account in simulations.

The percentage errors of FEA temperatures relative to SMAM's readings are shown in bars. All relative errors are less than 10%, indicating that simulations model thermal aspects of the motor with high fidelity.

B. FINITE ELEMENT ANALYSIS OF TORQUE AND RESISTIVE LOSSES OF THE INDUCTION MOTOR

The objective of using the finite element analysis is to make a thorough diagnosis of the electromagnetic behavior of the motor using a method that has no interference with the operation of the motor being analyzed. Using this method, it is able to extract the resistive losses in the stator armature as well as the torque via the Weighted Stress Tensor method [49].

This simulation is done considering the motor is operating under different levels of load conditions. As input current to the simulation, it is considered the steady state currents from 3A to 4A with an interval of 0.5A, as measured by SMAM. Fig. 13 shows the distribution of magnetic flux density (MFD) in the induction motor at load II (Fig. 12). As expected by theory, MFD is more intense in the stator's and rotor's ferromagnetic materials.

As mentioned before, torque results are obtained via the Weighted Stress Tensor method in FEMM how explained in the reference [49]. Fig. 14 shows the induction motor torque profile while varying the rotor angle by steps of 5 degrees. It can be observed that there is a maximum torque of 4.825N.m at 250 degrees and minimum value of 4.47N.m at 95 degrees. The curve presents an expected pattern of variation. Since the modelled motor has a cylindrical rotor (Fig. 13), the air-gap permeance is somewhat constant with rotation, causing the electromagnetic torque to oscillate by a relatively small amount around an average value [49].

Next, the electrical losses in the motor windings were analyzed as illustrated in Fig. 15. Considering that resistivity is directly influenced by temperature as shown in equation (12), it is expected that the resistive losses increase at each load level. Furthermore, for each load level, the steady state

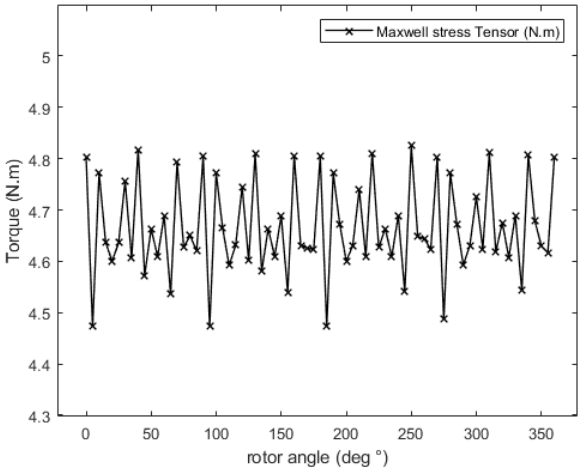

FIGURE 14. Simulated electromagnetic torque as a function of rotor angle for the induction motor considered in this work.

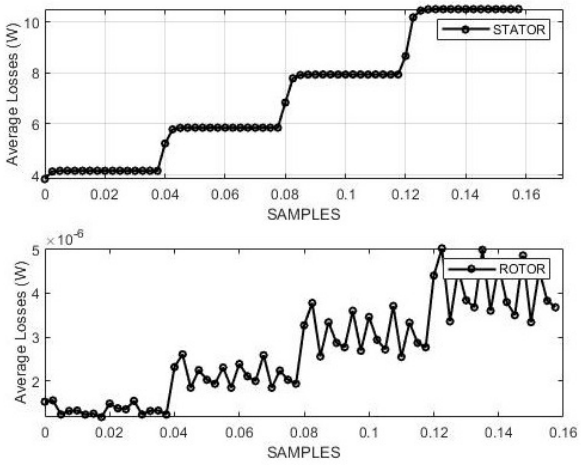

FIGURE 15. Average resistive losses per slot at stator and rotor across load levels.

current was simulated for a duration of 38 ms in order to verify that the losses are constant during that period.

Having obtained the losses in the windings, they were entered as input for thermal simulation, according to the strong coupling shown in Fig. 8. In order to validate the results, a FLIR thermographic camera (an infrared camera), temperature sensors on the thermal acquisition model and a thermocouple connected to a multimeter were used. The FEA performed by the software resulted in the temperature distribution illustrated in Fig. 16 for load level II. It is noticed that the copper strands are the points with highest temperature in both coils, as expected. An average temperature of 44°C in the motor is observed, which is in line with insulation class (F) as specified by the manufacturer.

In addition, it is possible to observe in Fig. 17 the average temperature graphs in the stator and rotor slots.

From this, it is noted that during the steady state time interval for each load level, the average temperature in the windings remains approximately constant. Furthermore, due to not taking into account the cooling effect from the motor's

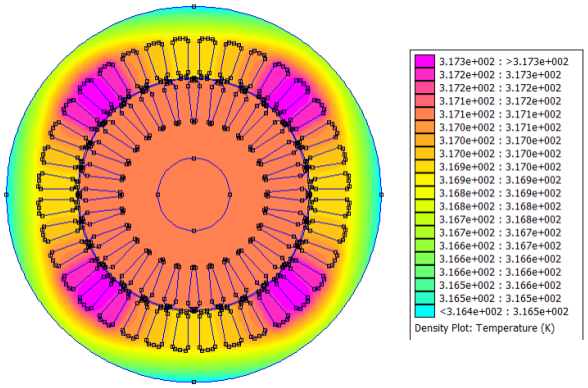

FIGURE 16. Temperature distribution (in Kelvin) in the motor.

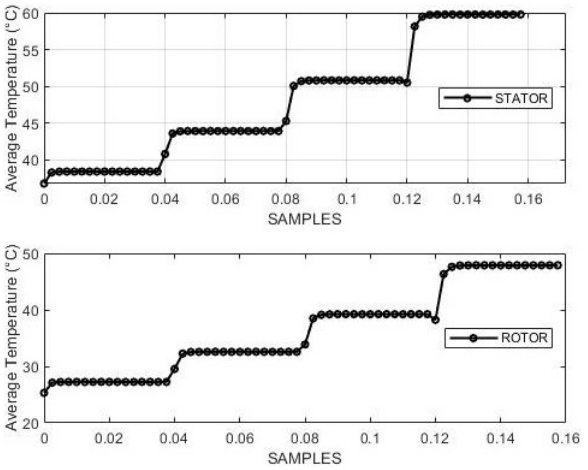

FIGURE 17. Average temperature in stator slot and rotor slot.

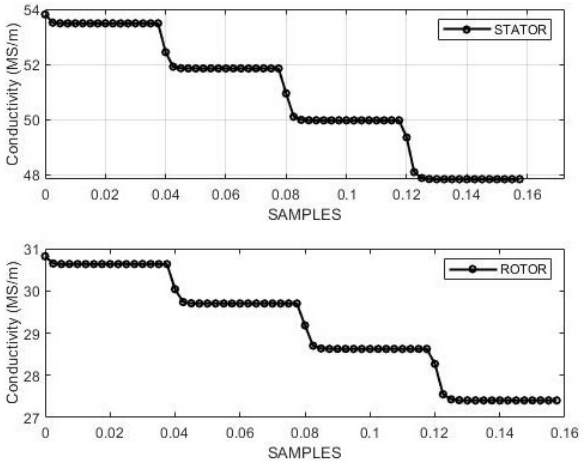

FIGURE 18. Electrical conductivity in the windings of the stator and rotor.

ventilator, the simulated temperature is above that measured by the sensors and infrared camera. This has greater importance as winding can reach temperatures harmful to insulation and decrease its service life [50].

Moreover, in view of the temperature obtained by the model, it is possible to calculate the conductivity of the

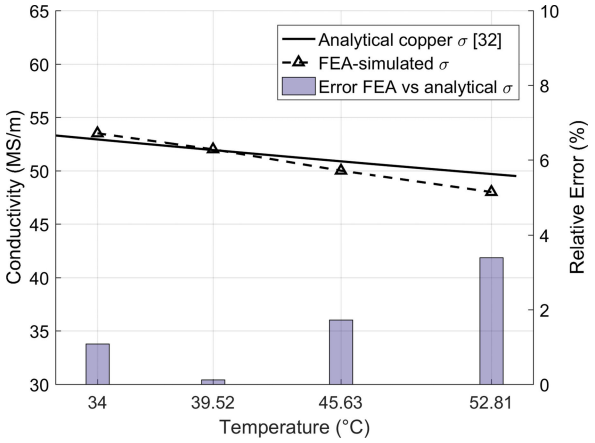

FIGURE 19. Algorithm for numerical simulations with strong thermo-magnetic coupling.

windings of the stator and rotor from (12). The results are presented in the graphs in Fig. 18.

In the graphs, it is observed that the conductivity values have variations for each current load level. In this case it is expected that there should be a reduction of the conductivity with the increase in temperature. This is further affirmed by [50], which proposed a design optimization of an axial-field eddy-current magnetic coupling based on magneto-thermal analytical model. As observed in Fig. 19, there is excellent agreement between the stator simulated conductivity and proposed by [50], with relative errors less than 4%, thus validating the results.

V. FINAL REMARKS

This paper deals with an application of the Industrial Internet of Things (IIoT) and computer simulations as tools for Digital Twin, with the aim of enabling a more detailed analysis of the induction motor. For this purpose, an IoT module is developed with sensors for measuring the motor's current and temperature. The measurements are entered into the FEMM software where strong coupled thermo-magnetic finite element analysis (FEA) is performed in order to enable the operator to understand the thermo-magnetic behavior of the motor in a non-invasive way, providing useful information for important tasks such as predicting potential failures.

The proposed system was used on an induction motor in a controlled environment. Commercial sensors were also installed to measure the same variables for comparison purposes. The motor's phase current and temperature in steady state measured by our system agreed very well with the readings of the commercial sensors, with relative errors less than 10%.

The measured current was entered as input to the FEA model. The temperature at the same point probed by sensors was calculated in the simulation; values were closely related to measurements (maximum error of 9.5%). Simulations also analyzed the temperature distribution, torque profile, resistive losses and stator copper conductivity, which are parameters very descriptive of the motor's operational state and that are

hard to measure, justifying the use of the DT concept. Those results presented behavior according to theory and similar to findings in literature, further validating the numerical model developed.

Therefore, the system presents a tool that can contribute to the predictive state monitoring of induction motors, since it presents consistent results in the permanent regime. Furthermore, the advance knowledge is very beneficial for the industry, as the motor is only stopped when needed for maintenance, reducing costs.

REFERENCES

[1] B. K. Tshoombe, J. F. D. Santos, R. C. F. Araujo, and W. D. S. Fonseca, "Implementation of DT-based monitoring system of induction motors," in *Proc. 14th IEEE Int. Conf. Ind. Appl. (INDUSCON)*, Aug. 2021, pp. 161–166.

[2] R. Saidur, "A review on electrical motors energy use and energy savings," *Renew. Sustain. Energy Rev.*, vol. 14, no. 3, pp. 877–898, Apr. 2010.

[3] S. Kumar, D. Mukherjee, P. K. Guchhait, R. Banerjee, A. K. Srivastava, D. N. Vishwakarma, and R. K. Saket, "A comprehensive review of condition based prognostic maintenance (CBPM) for induction motor," *IEEE Access*, vol. 7, pp. 90690–90704, 2019.

[4] A. J. Bazurto, E. C. Quispe, and R. C. Mendoza, "Causes and failures classification of industrial electric motor," in *Proc. IEEE ANDESCON*, Oct. 2016, pp. 1–4.

[5] O. E. Hassan, M. Amer, A. K. Abdelsalam, and B. W. Williams, "Induction motor broken rotor bar fault detection techniques based on fault signature analysis—A review," *IET Electr. Power Appl.*, vol. 12, no. 7, pp. 895–907, 2018.

[6] M. Gomes, P. C. Andrade, and T. Costa, "Análise de indicadores de desempenho da manutenção de um moinho de bolas," *Revista Thema*, vol. 15, no. 3, pp. 1089–1103, Aug. 2018.

[7] R. Jigyasu, A. Sharma, L. Mathew, and S. Chatterji, "A review of condition monitoring and fault diagnosis methods for induction motor," in *Proc. 2nd Int. Conf. Intell. Comput. Control Syst. (ICICCS)*, Jun. 2018, pp. 1713–1721.

[8] Z. M. Çınar, A. A. Nuhu, Q. Zeeshan, O. Korhan, M. Asmael, and B. Safaei, "Machine learning in predictive maintenance towards sustainable smart manufacturing in industry 4.0," *Sustainability*, vol. 12, no. 19, p. 8211, Oct. 2020.

[9] M. Compare, P. Baraldi, and E. Zio, "Challenges to IoT-enabled predictive maintenance for industry 4.0," *IEEE Internet Things J.*, vol. 7, no. 5, pp. 4585–4597, May 2020.

[10] K. Schwab, *The Fourth Industrial Revolution*. New York, NY, USA: Currency, 2017.

[11] F. Xia, L. Yang, L. Wang, and A. Vinel, "Internet of Things," *Int. J. Commun. Syst.*, vol. 25, no. 9, pp. 1101–1102, 2012.

[12] S. D. Milic and B. M. Babic, "Toward the future—Upgrading existing remote monitoring concepts to IIoT concepts," *IEEE Internet Things J.*, vol. 7, no. 12, pp. 11693–11700, Dec. 2020.

[13] S. Munirathinam, "Industry 4.0: Industrial Internet of Things (IIOT)," in *Advances in Computers*, vol. 117. Cambridge, MA, USA, 2020, pp. 129–164.

[14] Z. Jiang, Y. Guo, and Z. Wang, "Digital twin to improve the virtual-real integration of industrial IoT," *J. Ind. Inf. Integr.*, vol. 22, Jun. 2021, Art. no. 100196.

[15] Z. Zhang, J. Lu, L. Xia, S. Wang, H. Zhang, and R. Zhao, "Digital twin system design for dual-manipulator cooperation unit," in *Proc. IEEE 4th Inf. Technol., Netw., Electron. Autom. Control Conf. (ITNEC)*, Jun. 2020, pp. 1431–1434.

[16] W. S. Fonseca, D. S. Lima, A. K. F. Lima, M. V. A. Nunes, U. H. Bezerra, and N. S. Soeiro, "Analysis of structural behavior of transformer's winding under inrush current conditions," *IEEE Trans. Ind. Appl.*, vol. 54, no. 3, pp. 2285–2294, May 2018.

[17] L. Boscaglia, A. Boglietti, S. Nategh, F. Bonsanto, and C. Scema, "Numerically based reduced-order thermal modeling of traction motors," *IEEE Trans. Ind. Appl.*, vol. 57, no. 4, pp. 4118–4129, Jul. 2021.

[18] E. Glaessgen and D. Stargel, "The digital twin paradigm for future NASA and U.S. Air Force vehicles," in *Proc. 53rd AIAA/ASME/ASCE/AHS/ASC Struct., Struct. Dyn. Mater. Conf. 20th AIAA/ASME/AHS Adapt. Struct. Conf. 14th AIAA*, 2012, p. 1818.

[19] D. Jones, C. Snider, A. Nassehi, J. Yon, and B. Hicks, "Characterising the digital twin: A systematic literature review," *CIRP J. Manuf. Sci. Technol.*, vol. 29, pp. 36–52, May 2020.

[20] J.-F. Uhlenkamp, J. B. Hauge, E. Broda, M. Lutjen, M. Freitag, and K.-D. Thoben, "Digital twins: A maturity model for their classification and evaluation," *IEEE Access*, vol. 10, pp. 69605–69635, 2022.

[21] M. Liu, S. Fang, H. Dong, and C. Xu, "Review of digital twin about concepts, technologies, and industrial applications," *J. Manuf. Syst.*, vol. 58, pp. 346–361, Jan. 2021.

[22] N. Kardani, A. Zhou, M. Nazem, and S.-L. Shen, "Improved prediction of slope stability using a hybrid stacking ensemble method based on finite element analysis and field data," *J. Rock Mech. Geotech. Eng.*, vol. 13, no. 1, pp. 188–201, Feb. 2021.

[23] R. Minerva, G. M. Lee, and N. Crespi, "Digital twin in the IoT context: A survey on technical features, scenarios, and architectural models," *Proc. IEEE*, vol. 108, no. 10, pp. 1785–1824, Oct. 2020.

[24] P. F. S. de Melo and E. P. Godoy, "Controller interface for industry 4.0 based on RAMI 4.0 and OPC UA," in *Proc. II Workshop Metrol. Ind. 4.0 IoT (MetroInd4.0 IoT)*, Jun. 2019, pp. 229–234.

[25] D. Shyamala, D. Swathi, J. L. Prasanna, and A. Ajitha, "IoT platform for condition monitoring of industrial motors," in *Proc. 2nd Int. Conf. Commun. Electron. Syst. (ICCES)*, Oct. 2017, pp. 260–265.

[26] N. Khan, F. Rafiq, F. Abedin, and F. U. Khan, "IoT based health monitoring system for electrical motors," in *Proc. 15th Int. Conf. Emerg. Technol. (ICET)*, Dec. 2019, pp. 1–6.

[27] M. A. Fabrício, F. H. Behrens, and D. Bianchini, "Monitoring of industrial electrical equipment using IoT," *IEEE Latin Amer. Trans.*, vol. 18, no. 8, pp. 1425–1432, Aug. 2020.

[28] T. Y. Melesse, V. Di Pasquale, and S. Riemma, "Digital twin models in industrial operations: State-of-the-art and future research directions," *IET Collaborative Intell. Manuf.*, vol. 3, no. 1, pp. 37–47, Mar. 2021.

[29] L. Zhao, I. Matsuo, Y. Zhou, and W.-J. Lee, "Design of an industrial IoT-based monitoring system for power substations," in *Proc. IEEE/IAS 55th Ind. Commercial Power Syst. Tech. Conf. (ICPS)*, May 2019, pp. 1–6.

[30] S. Venkatesan, K. Manickavasagam, N. Tengenkai, and N. Vijayalakshmi, "Health monitoring and prognosis of electric vehicle motor using intelligent-digital twin," *IET Electr. Power Appl.*, vol. 13, no. 9, pp. 1328–1335, 2019.

[31] S. J. Salon, *Finite Element Analysis of Electrical Machines*. Boston, MA, USA: Kluwer, 1995.

[32] M. Popescu, D. Dorrell, and M. McGilp, "Instantaneous electromagnetic torque estimation in electrical motors using the finite element method—A review," *Proc. 17th ICEM*, 2006, pp. 1–6.

[33] M. Sadiku, *Elements of Electromagnetics*. New York, NY, USA: Oxford Univ. Press, 2018.

[34] YHDC. (2015). *Split Core Current Transformer Model SCT013-100 Datasheet*. Accessed: Mar. 25, 2022. [Online]. Available: https://en.yhdc.com/comp/file/download.do?id=941

[35] *Electromagnetic Compatibility (EMC)—Part 4–30: Testing and Measurement Techniques—Power Quality Measurement Methods*, IEC Standard 61000-4-30:2015/AMD1:2021, International Electrotechnical Commission, Geneva, Switzerland, 2021.

[36] CANTHERM. (2012). *Pearl-Shaped Precision NTC Thermistor for Temperature Measurement*. Accessed: Oct. 1, 2022. [Online]. Available: https://www.cantherm.com/wp-content/uploads/2017/05/cantherm_mf52_1.pdf

[37] S. Calzavara, R. Focardi, M. Nemec, A. Rabitti, and M. Squarcina, "Postcards from the post-HTTP world: Amplification of HTTPS vulnerabilities in the web ecosystem," in *Proc. IEEE Symp. Secur. Privacy (SP)*, May 2019, pp. 281–298.

[38] N. Nurseitov, M. Paulson, R. Reynolds, and C. Izurieta, "Comparison of JSON and XML data interchange formats: A case study," *Caine*, vol. 9, pp. 157–162, Nov. 2009.

[39] B.-H. Lee, E. K. Dewi, and M. F. Wajdi, "Data security in cloud computing using AES under HEROKU cloud," in *Proc. 27th Wireless Opt. Commun. Conf. (WOCC)*, Apr. 2018, pp. 1–5.

[40] Espressif Systems. (2022). *ESP32-WROOM-32D & ESP32-WROOM-32U Datasheet*. Accessed: Mar. 25, 2022. [Online]. Available: https://www.espressif.com/sites/default/files/documentation/esp32-wroom-32d_esp32-wroom-32u_datasheet_en.pdf

[41] E. Batista, N. Citadin, M. Marin, M. R. Barghouti, and E. M. O. Lopes, "Um sistema experimental de código aberto para pesquisa em controle ativo de vibrações," in *Proc. XXXVIII Simpósio Brasileiro Telecomunicações Processamento Sinais (SBRT)*, 2022, pp. 1–5.

[42] E. J. T. Pereira, D. A. Guimarães, and C. S. Fonseca, "Sensoriamento espectral via modo adaptativo de saltos em frequência do Padrão Bluetooth," in *Proc. XXXVIII Simpósio Brasileiro Telecomunicações Processamento de Sinais (SBRT)*, 2020, pp. 1–5.
[43] D. V. Hutton, *Fundamentals of Finite Element Analysis*. New York, NY, USA: McGraw-Hill, 2004.
[44] J. W. R. Borges, W. D. S. Fonseca, F. D. S. Brasil, and R. C. F. Araújo, "Steady-state multiphysics analysis of stator bar using finite element method," *Int. J. Appl. Electromagn. Mech.*, vol. 65, no. 3, pp. 513–526, Mar. 2021.
[45] D. Meeker. (2020). *Finite Element Method Magnetics—Version 4.2 User's Manual*. Accessed: Mar. 25, 2022. [Online]. Available: https://www.femm.info/wiki/Files/files.xml?action=download&file=manual.pdf
[46] J. P. Bastos, M. F. R. R. Cabreira, N. Sadowski, S. R. Arruda, and S. L. Nau, "A thermal analysis of induction motors using a weak coupled modeling," *IEEE Trans. Magn.*, vol. 33, no. 2, pp. 1714–1717, Mar. 1997.
[47] Y. Wang, S. Li, and W. Meng, "Strong coupling analysis of fluid–solid for magnetorheological fluid braking system," *J. Intell. Mater. Syst. Struct.*, vol. 29, no. 8, pp. 1586–1599, May 2018.
[48] J. M. Tabora, B. K. Tshoombe, W. S. Fonseca, M. E. L. Tostes, E. O. Matos, U. H. Bezerra, and M. O. Silva, "Virtual modeling and experimental validation of the line-start permanent magnet motor in the presence of harmonics," *Energies*, vol. 15, no. 22, p. 8603, 2022.
[49] M. Popescu, D. Dorrell, and M. McGilp, "Instantaneous electromagnetic torque estimation in electrical motors using the finite element method—A review," in *Proc. 17th ICEM*, 2006, pp. 1–6.
[50] J. Fontchastagner, T. Lubin, S. Mezani, and N. Takorabet, "Design optimization of an axial-field eddy-current magnetic coupling based on magneto-thermal analytical model," *Open Phys.*, vol. 16, no. 1, pp. 21–26, 2018.

JHENNIFER F. DOS SANTOS graduated in microcomputer maintenance from the Instituição Salesiana do Trabalho, with experience in computer maintenance. She is currently pursuing the degree in electrical engineering with the Federal University of Pará (UFPA). She is also in a scholarship at the Laboratory of Design and Analysis of Electromechanical Devices (LCADE), Center of Excellence in Energy Efficiency in the Amazon (CEAMAZON), where she develops and research on the Internet of Things in Industry (IIoT), electric motors, automation of industrial processes, predictive maintenance, and energy efficiency.

BENDICT K. TSHOOMBE is currently pursuing the master's degree in electrical engineering with the Graduate Program in Electrical Engineering, Federal University of Pará (UFPA). He is also a member of the Laboratory for Design and Analysis of Electrical Devices (LCADE), working on the thermo-magnetic analysis of electrical equipment. His research interests include thermo-magnetic analysis of electrical equipment, the Industrial Internet of Things, finite element method (FEM), and electrical installation in naval vessels.

LUCAS H. B. SANTOS is currently pursuing the degree in biomedical engineering with the Federal University of Pará (UFPA). He is also a Technician in electrotechnics at IFPA. He is a fellow at the Laboratory for Design and Analysis of Electromechanical Devices (LCADE) in the Automatic Ambu-Actuator (AAA) Project, which has a partnership with the company Hydro-AlunoNorte. In addition, it is part of a developed patent that uses the Internet of Things (IoT), electronic circuitry, and electrical material to preserve vaccines and biological samples. He is a Designer of on-grid photovoltaic systems using AutoCad software, and has experience with residential installation. His main research interests include biomedical instrumentation, health 4.0, renewable energy, and electrical installations.

RAMON C. F. ARAÚJO received the bachelor's, master's, and Ph.D. degrees in electrical engineering from the Federal University of Pará (UFPA), in 2013, 2015, and 2020, respectively. His doctorate was about developing a machine-learning-based automatic partial discharge recognition system for the condition monitoring of hydro-generators. Currently, he is working as a Postdoctoral Researcher in a research and development project with a private oil and gas company in the area of seismic signal processing for oil reservoir monitoring. He has experience in the areas of digital twin, the Internet of Things, magneto-hydrodynamics, partial discharges, machine learning, grounding systems, numerical methods, high performance computing, and radar systems.

ALLAN R. A. MANITO received the bachelor's degree in electrical engineering and the master's and Ph.D. degrees in electrical engineering in the area of power systems from the Federal University of Pará (UFPA), in 2006, 2009, and 2019, respectively. He works as a Professor at the School of Electrical and Biomedical Engineering, UFPA. His main research interests include high voltage, power quality, and energy efficiency.

WELLINGTON S. FONSECA received the bachelor's degree in physics and the master's and Ph.D. degrees in electrical engineering from the Federal University of Pará (UFPA), in 2007, 2010, and 2016, respectively, and the Postdoctoral degree from COPPE-UFRJ, in 2019. He has been a Professor at UFPA, since 2011. He is currently a Professor at the Institute of Technology of the Federal University of Pará–ITEC/FEEB. He is also a Researcher at the Center of Excellence in Energy Efficiency in the Amazon (CEAMAZON). He is a Professor of the Graduate Program in Mechanical Engineering (PPGEM) and the Graduate Program in Electrical Engineering (PPGEE). He is a Reviewer of journals and scientific events, such as *International Journal of Applied Electromagnetics and Mechanics*, the IEEE Access, IEEE/IAS International Conference on Industry Applications (INDUSCON), and *Journal of Studies and Research on Technological Education*. He has experience in the areas of energy, principles of industry 4.0, low frequency electromagnetism, interactions between electromagnetic and mechanical phenomena, electrical materials, finite element method, and finite volume method.

MARCELO O. SILVA received the B.Sc. and master's degrees in mechanical engineering from the Federal University of Pará, Belém, Brazil, in 2000 and 2002, respectively, and the Ph.D. degree in mechanical sciences from the Federal University of Rio de Janeiro, Brazil, in 2007. He has experience in mechanical engineering, with emphasis on fluid mechanics, working mainly on the following topics: natural convection, biphasic flow, abrupt expansion, electroresistive sensor technique, limit layer, asymptotic analysis, pneumatic transport, and experimental techniques.